ELSEVIER

Chemical Engineering Journal 90 (2002) 219–229

Chemical Engineering Journal

www.elsevier.com/locate/cej

Experimental evaluation of photon absorption in an aqueous TiO_2 slurry reactor

M. Salaices, B. Serrano, H.I. de Lasa*

Faculty of Engineering Science, Chemical Reactor Engineering Center, University of Western Ontario, London, Ont., Canada N6A B9

Received 7 December 2001; accepted 6 February 2002

Abstract

This study presents an experimental evaluation of photon absorption in a TiO_2 slurry medium using an annular photoreactor. This photoreactor was equipped with several windows placed at equidistant axial positions. Tubular black collimators and inner polished-aluminum collimators were attached to these windows to measure the total transmitted radiation and the transmitted non-scattered radiation. Experiments were developed with six TiO_2 commercial powders having differences in particle size, agglomerate particle size in water suspension, and specific surface area.

Modeling allowed to establish that the forward-transmitted radiation can be represented by the difference of two exponential decay functions accounting respectively for the total transmitted radiation and the transmitted non-scattered radiation. These two exponentials are functions of particle concentration and extinction coefficients, with the extinction coefficient for the transmitted radiation being strongly affected by the particle agglomerate size.

Keywords: Phenol photodegradation; Photon absorption; Extinction coefficients; Quantum efficiencies

1. Introduction

Heterogeneous photocatalysis has been a very active area of research in recent years with more than 700 papers published only in the area of water purification. however, in order to achieve further progress in photocatalysis, it is very important to use and define fundamentally based efficiency parameters allowing the comparison of experimental results, obtained from different laboratories, under different experimental conditions.

Thus, several efficiency definitions were already advanced in the technical literature:

(a) The quantum yield (QY), defined as the number of radicals produced on the catalyst surface during the primary reaction processes per photon absorbed [1,2]. Whereas, QY is one of the most frequently used parameters to describe photochemical activity [3–6] there are still discrepancies between authors about the proper application of its definition. Frequently, the QY is based on the rate of incident photons reaching the internal reactor walls. In such cases, the estimated QY represents an apparent QY or the lower limit for that parameter.

(b) The photonic efficiency describing the number of reactant molecules transformed or product molecules formed over the number of incident photons on the reactor cell [7]. This parameter is related to a standard process with fixed reactor geometry, light source, and photocatalyst properties.

(c) The quantum efficiency, defined as the ratio of the number of molecules of product formed to the total number of photons absorbed, is employed when the lamp emission spectrum is unknown.

(d) The relative photonic efficiency defined as the ratio between the actual QY and the QY for the photocatalyzed oxidative disappearance of phenol using Degussa P25 catalyst, as the standard catalyst [7,8].

(e) The photochemical thermodynamic efficiency factor (PTEF) describing the fraction of the photon energy utilized for the generation of hydroxyl radical groups [9].

(f) The electrical energy per order (EE/O) defined as the electrical energy used to reduce the concentration of a pollutant by one order of magnitude in 1000 US gallons (3787 l) of water [10].

(g) The energetic efficiency of degradation (EED) expressed as the amount in ppm ($mg\,l^{-1}$) of organic carbon, contained in a given solution volume, per kWh of electrical energy used for its irradiation [8].

* Corresponding author. Tel.: +1-519-661-2144; fax: +1-519-661-3498.
E-mail address: hdelasa@eng.uwo.ca (H.I. de Lasa).

1385-8947/02/$ – see front matter © 2002 Elsevier Science B.V. All rights reserved.
PII: S1385-8947(02)00037-2

Nomenclature

c	speed of light ($m\,s^{-1}$)
C	catalyst concentration ($g\,l^{-1}$)
d_a	average agglomerate size (nm)
d_p	volume-equivalent particle diameter (nm)
d_p^*	volume-equivalent particle diameter estimated from S_a (nm)
d_{pr}	particle diameter range (nm)
h	Planck's constant (J s)
H	reactor height (cm)
L_l	lamp length (cm)
P_a	rate of absorbed photons (einstein s^{-1})
$P_{a\text{-wall}}$	rate of photons absorbed and back-reflected by the inner cylinder wall (einstein s^{-1})
P_{bs}	rate of back-scattered photons exiting the system (einstein s^{-1})
$P\|_{C\to 0^+}$	rate of photons transmitted when catalyst concentration approaches to zero from the right hand side of the d_p/d_C discontinuity (einstein s^{-1})
P_{fs}	rate of photons forward-scattered by the slurry (einstein s^{-1})
P_i	rate of photons reaching the reactor inner surface (einstein s^{-1})
P_{ns}	rate of transmitted non-scattered photons (einstein s^{-1})
P_o	rate of photons emitted by the lamp (einstein s^{-1})
P_t	rate of photons transmitted (einstein s^{-1})
$q(\theta, z, \lambda)$	radiative flux ($J\,s^{-1}\,m^{-3}$)
$q_{ac}(\theta,z)$	radiative flux as detected using the aluminum collimator ($J\,s^{-1}\,m^{-2}$)
$q_{bc}(\theta, z)$	radiative flux as detected using the black collimator ($J\,s^{-1}\,m^{-2}$)
r	radial coordinate (m)
R_i	radial coordinate corresponding to the outer surface of the inner Pyrex glass cylinder (cm)
R_l	radial coordinate corresponding to lamp surface (cm)
R_o	radial coordinate corresponding to inner surface of the outer cylinder (cm)
R_w	radial coordinate corresponding to the window inner surface, located on the outer cylinder (cm)
R^2	least-squares regression coefficient
S_a	specific surface area ($m^2\,g^{-1}$)
z	axial coordinate or reactor height (m)

Greek letters

α	apparent extinction coefficient ($l\,g^{-1}$)
β	true extinction coefficient ($l\,g^{-1}$)
β_s	specific extinction coefficient ($cm^2\,g^{-1}$)
η	lamp efficiency (%)
λ	radiation wavelength (m)
θ	angle in cylindrical coordinates (rad)

It has to be pointed out that the above mentioned definitions employ a common variable, except for the EE/O and the EED, the rate of photons absorbed by the photocatalyst. Thus, it is in the accurate measurement of the rate of absorbed photons that rests to a significant extent, the meaningfulness definition of these efficiency parameters.

Regarding the absorbed photons in TiO_2 suspensions, this is a function of: (i) reactor geometry; (ii) catalyst concentration [11]; (iii) particle agglomerate size [12,13]; (iv) pH; (v) recycle flow rate [14]; and (vi) radiation wavelength [5,14].

Several approaches have been followed to evaluate the rates of absorbed photons. The simplest method considers that the reactor medium absorbs all photons reaching the reactor wall (incoming side). In this respect, the flux of photons is determined by radiometric measurements or chemical actinometry. This method gives lower efficiencies than the true values since the extent of light scattered in the solid catalyst suspension is not considered. Other approaches use an apparent extinction coefficient obtained by actinometric measurements of the light transmitted through a stirred TiO_2 suspension [6,15]. More complex approaches obtain the rate of absorbed photons solving the radiation transfer equation for a given reactor configuration with a limited number of assumptions [16].

In this work, an experimental method was used for the determination of the rate of absorbed photons in an aqueous TiO_2 slurry tubular reactor evaluating the radiation transmitted through the reactor medium by radiometric measurements. The approach of the present study also allows a quantitative assessment of the forward and backward scattering radiation and of the extinction coefficients. The value of this methodology was demonstrated in a recent contribution when studying the photocatalytic conversion of phenol [17].

2. Experimental methods

The experimental system used was constituted by the following components (Fig. 1):

(a) A batch-recycle unit with a 2.5 l tubular concentric reactor (42 cm length, 8.9 cm diameter outer cylinder, and 3.5 cm diameter inner cylinder) and a 3.5 l well stirred tank.
(b) A TiO_2 slurry suspension circulating between the annular space of two concentric cylinders (2.7 cm).
(c) A 15 W black-light blue lamp (UVP-XX-15BLB, located in the central channel of the reactor (2.54 cm × 40 cm; diameter × length). The lamp has a spectral energy distribution in the 300–405 nm wavelength region.

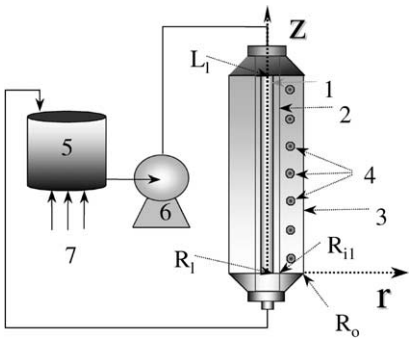

Fig. 1. Schematic representation of a batch-recycle photocatalytic unit. (1) Black-light blue lamp, (2) Pyrex glass inner cylinder, (3) black-polyethylene outer cylinder, (4) fused silica windows, (5) stirred tank, (6) centrifugal pump, and (7) air injection.

(d) A plastic centrifugal pump allowing the recirculation of the TiO_2 suspension at different flow rates (0–16 l min^{-1}).

Regarding the reactor itself, its inner cylinder was made out of Pyrex glass (2.25 mm in thickness) to allow the transmission of most of the UV radiation emitted by the lamp. The outer cylinder was made of non-reflecting black polyethylene. This non-reflecting material was chosen to eliminate the radiation reaching the reactor inner surface wall that could be reflected towards the sensor cell. Seven 1.1 cm diameter (0.325 cm thick) circular fused silica windows were equally spaced (6.4 cm) along the reactor outer cylinder wall. Table 1 summarizes the most important characteristics of the reactor system used in this study.

Radiation measurements were made at each window position using an UVX digital radiometer equipped with a circular 0.9 cm diameter sensor cell (UVX-365). With the help of tubular polished-aluminum and tubular black collimators (1.0 cm × 2.3 cm and 1.0 cm × 9.2 cm, inner diameter × length, respectively), it was possible to control the amount of radiation reaching the sensor cell and to fix the position between the sensor cell and the reactor. Tubular black collimators were used to determine the suspension extinction coefficients since their non-reflective surface minimizes the forward-scattered radiation that reaches the detector. Tubular polished-aluminum collimators were used to assess the total transmitted radiation through the slurry.

Table 1
Photocatalytic reactor and lamp characteristics

Component	Parameter	Values
Annular reactor	R_i (cm)	1.74
	R_o (cm)	4.45
	H (cm)	44
Inner cylinder	Thickness (cm)	0.225 cm
Lamp (black-light blue lamp)	Nominal input power (W)	15
	h (%)	15–20
	L_l (cm)	40
	R_l (cm)	1.25
	Characteristic emission	Isotropic and superficial
	Emission range (nm)	300–405
	Emission rate (einstein s^{-1})	1.057×10^{-5}
Windows (fused silica)	Diameter (cm)	1
	Thickness (cm)	0.325

Lamps were calibrated using an auxiliary equipment called lamp testing unit (LTU) [9]. This unit is constituted by a lamp holder with inner surface painted in black and a rail with 1 cm opening extending through the length of the lamp. The UVX-365 sensor was displaced through this rail at a fixed distance from the light source.

A series of runs were performed with six TiO_2 catalysts: (a) Anatase 1 (Aldrich, Cat. 24,857-6, lot 04811KR, >99% anatase); (b) Anatase 2 (Aldrich, Cat. 23,203-3, lot 07627BX, 99.9% anatase); (c) Hombikat (Fluka, lot 380681/142599, anatase modification); (d) P25 (Degussa CN: 1610); (e) Rutile 1 (Aldrich, Cat. 20,475-7, lot 10801HS; and, (f) Rutile 2 (Aldrich, Cat. 22,422-7, lot 16126CY). For each one of these catalysts, the transmitted radiation through the slurry was measured at each window position for different catalyst concentrations and several recycle flow rates. Deionized water was used in all cases.

Primary particle size range, d_{pr}, was estimated using scanning electron microscope micrographs of the catalyst samples (Hitachi model S-4500 Solid Emission SEM). Typical values of these measurements and the corresponding volume-equivalent diameters, d_p, based on the micrographs are reported in Table 2. Regarding Hombikat catalyst, a d_p based on the SEM micrographs could not be obtained. The Hombikat sample studied was formed (micrograph not shown) by irregular thin filaments of 20 nm wide and 70–400 nm long.

Concerning particle agglomeration of solid powders dispersed in water, it was determined in a laser light scattering system (Brinkmann, PSA 2010). Samples of the catalyst slurry were taken from the reactor at several intervals during the transmission measurements and analyzed for the particle agglomerate size. This procedure ensures that measurements of agglomerate size were taken at the same operating conditions maintained during the radiation transmission measurements. Gentle stirring was used to maintain the suspension of the catalyst during the analyses. Values of these measurements are reported in Table 2. It is shown that all catalysts considered in the present study display significant particle agglomeration. For instance, Degussa P25 samples showed a d_a/d_p ratio as large as 42 times whereas d_a/d_p ratios for the other catalysts were restricted in the 4–7 range. Thus, it can be observed that there is large agglomeration in the case of the small particle catalysts such as Hombikat and Degussa P25. In addition, particle agglomeration in sizes of at least two times larger than the wavelengths of the incident radiation ($\bar{\lambda}_{300}^{410} \approx 348$ nm) allows the application of geometric optics for the treatment of the radiation transfer through the slurry media [18].

Table 2
Physical properties of various titanium dioxide samples

Sample	d_{pr} (nm)	d_p (nm)	d_a (nm)	d_a/d_p	S_a ($m^2\,g^{-1}$)	d_p* (nm)
Anatase 1	80–180	134	750	6	10.5	147
Anatase 2	100–200	146	1050	7	12.2	126
Hombikat	10–70	–	1540	–	250	7
P25	20–60	32	1340	42	54	29
Rutile 1	300–900	496	2300	5	2.9	490
Rutile 2	160–1060	576	2400	4	2.2	632

* Estimated from the specific surface area measurements.

The catalyst specific surface areas, S_a, were measured in a Micrometrics Analyzer (TPD/TPR model 2900), outgassing for 120 min at 250 °C. S_a values are also reported in Table 2. For all catalyst analyzed, the Hombikat variety showed the largest specific surface area approximately five times larger than that of Degussa P25, 22 times larger than that for Anatase 1 and 2 catalysts, and 100 times larger than that of Rutile 1 and 2 samples. Anatase 1 and 2 showed similar S_a values around $10\,m^2\,g^{-1}$ whereas Rutile 1 and 2 samples displayed specific surface areas around $2.5\,m^2\,g^{-1}$.

Using the S_a values determined above, volume-equivalent diameters, d_p^*, were determined for all the catalysts. The d_p^* values are included in the last column of Table 2. Note that for all cases, except for Hombikat, d_p^* values fall between ±14% of d_p determined by SEM. Regarding Hombikat sample, the d_p^* value estimated from S_a was found to be 7 nm. Thus, Hombikat is the catalyst with the smallest d_p studied followed by Degussa P25, Anatase 1 and Rutile 1 and 2. Rutile 2 provided as well, as reported in Table 2 the largest spread in particle sizes.

3. Radiation transmission modeling

The rate of absorbed photons was estimated using a macroscopic radiant energy balance with this balance applied to a control volume with boundaries containing the slurred catalyst:

$$P_a = P_i - P_{bs} - P_t \tag{1}$$

with P_a being the rate of absorbed photons, P_i the rate of photons reaching the reactor inner surface, P_{bs} the rate of back-scattered photons exiting the system, and P_t is the rate of transmitted photons. All terms are in einstein s^{-1}.

Concerning the various terms in Eq. (1), they can be estimated as follows:

(a) P_i or the rate of photons reaching the reactor inner surface can be determined from P_o, the rate of photons emitted by the lamp minus $P_{a\text{-wall}}$ the rate of photons absorbed or back-reflected by the inner cylinder wall. That is,

$$P_i = P_o - P_{a\text{-wall}} \tag{2}$$

with the rate of photons emitted by the lamp determined as follows:

$$P_o = \frac{\bar{\lambda}}{hc}\int_{\lambda_1}^{\lambda_2}\lambda\int_0^{\infty}\int_0^{2\pi} q(\theta, z, \lambda) r\,d\theta\,dz\,d\lambda \tag{3}$$

where $q(\theta, z, \lambda)$ is the radiative flux ($J\,s^{-1}\,m^{-3}$), λ the radiation wavelength (m), r the radial coordinate (m), z the axial coordinate (m), h the Planck's constant (J s), and c the speed of light ($m\,s^{-1}$).

Note that $q(\theta, z, \lambda)$ can be determined by means of radiometric measurements in the LTU and from the lamp emission spectrum. The radiative flux integrated over the wavelength $q(\theta, z)$ was modeled by the use of an extensive source with superficial diffuse emission model (ESSDEM) [19]. One additional parameter, the lamp efficiency η, was included in the model to account for lamp inefficiencies and the lamp intensity decay with time.

(b) $P_{a\text{-wall}}$ was estimated in the LTU on the basis of radiation transmission measurements through the inner cylinder.

(c) P_{bs} or the rate of back-scattered photons exiting the system, was approximated from the difference between P_i and the rate of photons transmitted when the catalyst concentration approaches to zero ($P|_{C\to 0^+}$) [15,20].

$$P_{bs} = P_i - P|_{C\to 0^+} \tag{4}$$

The use of Eq. (4) incorporates two assumptions: (i) the back-scattered photons exiting the system are those related to a number of back-scattering centers located in a boundary layer of particles very close to the inner cylinder wall; and (ii) once a maximum number of scattering centers is reached in this boundary layer, there is no additional back-scattering of photons leaving the system.

(d) P_t or the rate of transmitted photons represents the addition of the transmitted non-scattered radiation and the forward-scattered radiation:

$$P_t = P_{ns} + P_{fs} \tag{5}$$

Regarding P_{fs}, it can be estimated from the difference between the measured radiation, evolving through the slurry using the tubular polished-aluminum collimator, and the measured radiation using the tubular black collimator. It has to be stressed that the polished-aluminum collimators

account for the combined transmitted non-scattered radiation and forward-scattering radiation whereas the tubular black collimators account for the transmitted non-scattered radiation only.

Thus, from Eq. (5), it results

$$P_{fs} = P_t - P_{ns} \quad (6)$$

4. Analysis and discussion of results

A first step, in the present study, was the characterization of the lamp in the LTU with the help of a radiometer placed at a fixed distance from the light source. Fig. 2 shows a typical radiative flux distribution $q(\theta, z)$ in mW cm^{-2} at two radial positions. It is important to mention that whereas most of the characterized BLB lamps showed quite symmetric radiation distributions, few of the lamps after more than 1000 h of operation presented asymmetric radiation distributions along the axial coordinate. In this respect, special care was taken to use in the experiments of the present study, lamps displaying symmetric radiation distributions. Then, for cases like the one of Fig. 2, the radiative flux distribution $q(\theta, z)$ determined in the LTU and the lamp emission spectrum was used for calculating P_o (refer to Eq. (3)).

Regarding $q(\theta, z)$, it was modeled by the use of an extensive source with superficial diffuse emission model (ESSDEM). Both lamp efficiency and lamp intensity decay with time were assessed considering the ratio between P_o (Eq. (3)) and the lamp nominal power. Lamps used in this study displayed efficiencies in between 15 and 20%. The model considered was tested, as described in Fig. 2 at two radial positions: 3.1 and 4.5 cm from the lamp axis (or 1.88 and 3.23 cm from the lamp surface).

Application of Eq. (1) requires the determination of P_i and $P_{a\text{-wall}}$ parameters. Again, using the LTU, it was possible to calculate $P_{a\text{-wall}}$ and consequently to establish that the radiation transmitted to the inner cylinder was about 96% of the radiative flux ($P_i = 0.958 P_o$) with this parameter being independent of the axial reactor position. Negligible radiation losses were assumed in the space between the lamp surface and the inner cylinder surface. The calculated average extinction coefficient for the inner cylinder material was 0.70 cm^{-1} in the 400–300 nm wavelength range.

Fig. 3 illustrates the radiative flux distribution in an empty annular reactor, as predicted by the ESSDE model. The radiation attenuation by the inner cylinder wall is included. This figure allows the calculation of P_i for the case of the present study (reactor inner surface located at 1.74 cm from the lamp axis). To achieve this, the function $q(\theta, z)$ was integrated over both the θ angle and the z coordinate, at a fixed 1.74 cm radial distance, with this distance being the one defining the reactor inner surface. The rate of photons emitted by the lamp, P_o, and the rate of photons reaching the reactor surface P_i, were determined as 1.057×10^{-5} and 1.01×10^{-5} einstein s^{-1}, respectively.

Once P_i was determined, systematic measurements of the transmitted radiation at each window position were performed in the reactor (Fig. 1) and this for each one of the six catalysts. This was done at various catalyst concentrations and flow rates using both the tubular polished-aluminum and the black collimators.

Fig. 4 displays the values of transmitted radiation, P_t, at a radial position 7.62 cm with respect to the reactor axis, for Degussa P25 catalyst as measured using the radiometer and the tubular polished-aluminum collimators placed at the different reactor windows. This figure reports several catalyst concentrations with experiments developed at a flow rate of

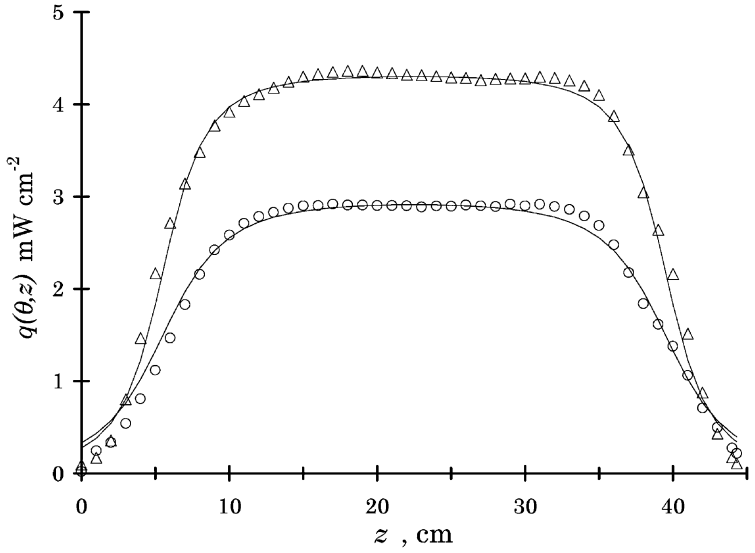

Fig. 2. Lamp axial radiative flux distribution measured at two radial positions: (△) 3.1 cm, and (○) 4.5 cm. Solid lines represent an ESSDE model evaluated at the same radial positions.

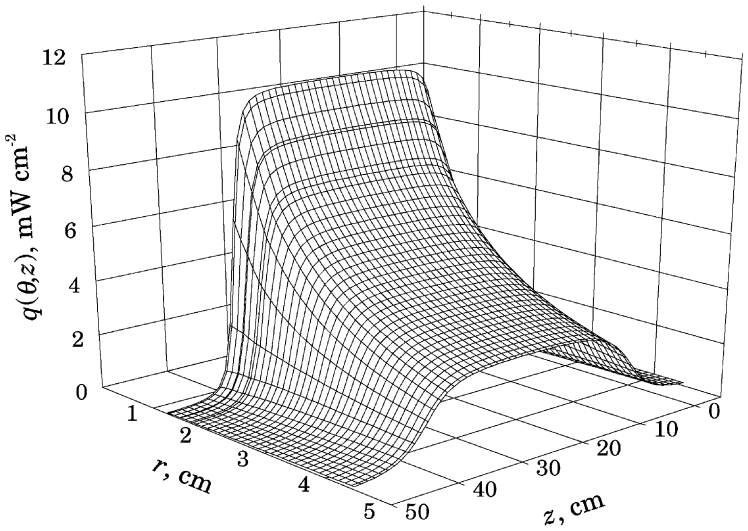

Fig. 3. Radiative flux distribution in an empty annular reactor.

$12\,l\,min^{-1}$. It can be observed that in the central region of the reactor, from 10 to 36 cm axial length, the axial radiation profile develops with essentially no changes of radiation levels. It is in this region where it is postulated that end effects of the set up are negligible and consequently where radiation transmission measurements are more reliable. It can also be observed, in this figure, that this uneven light distribution tends to moderate when the particle concentration is increased. This is a result of the growing influence of particle light scattering and yields as a consequence a smoothing of reactor end effects.

Fig. 5a and b show the normalized radiative flux evolving though the slurry versus the catalyst concentration for each one of the six catalysts studied as measured by the polished-aluminum and black collimators, respectively. A normalization factor was used ($10^3/q_{ac0}$) in order to improve the data visualization and facilitate the comparison of results. These measurements were performed at the radial positions of 7.62 and 16.8 for the polished-aluminum and the black collimators, respectively. It can be noticed that the transmitted radiation decreases with catalyst concentration, following essentially for all cases a decreasing exponential with catalyst concentration: $q_{ac}(\theta, z) = q_{ac}(\theta, z)|_{C\to 0^+}\, e^{-\alpha C}$ and $q_{bc}(\theta, z) = q_{bc}(\theta, z)|_{C\to 0^+}\, e^{-\beta C}$

Thus, given the suitability of the exponential decay model fitting, obtained with a high degree of correlation

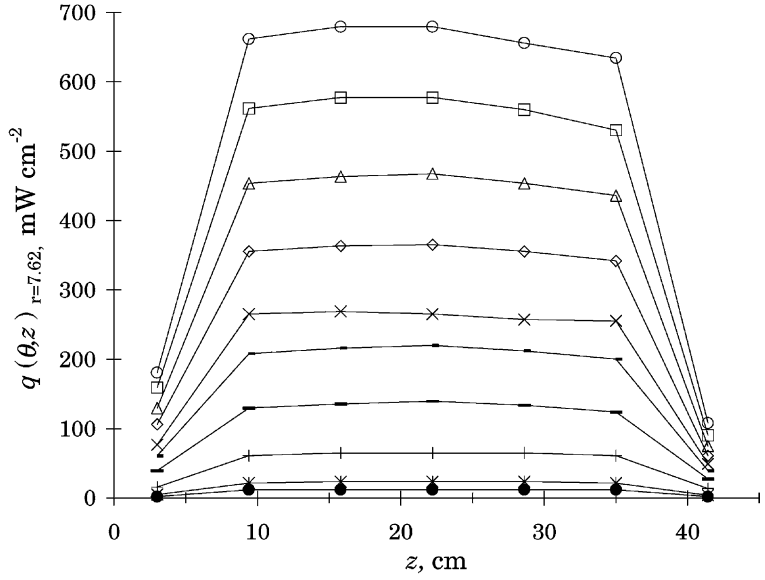

Fig. 4. Axial transmitted radiation distribution as a function of catalyst concentration for Degussa P25. Concentrations in $mg\,l^{-1}$. (○) 0, (□) 3, (△) 5, (◇) 10, (×) 15, (- - -) 20, (—) 30, (+) 50, (✳) 80, (●) 100.

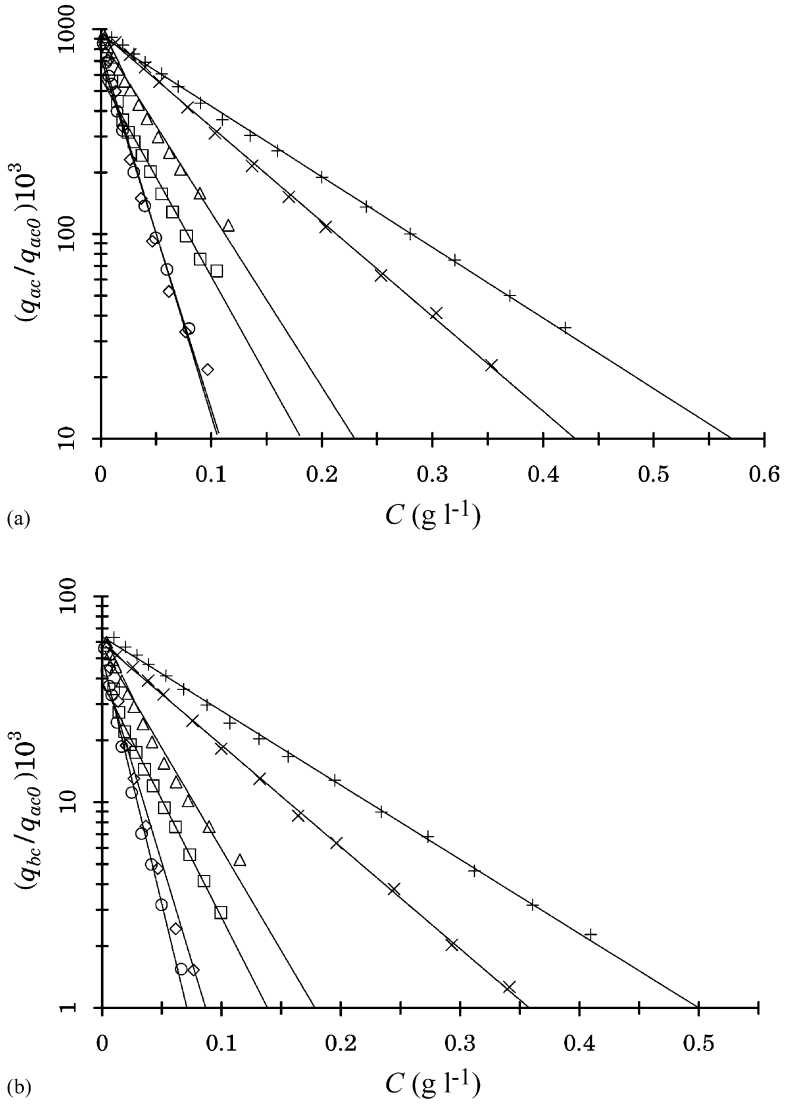

Fig. 5. (a) Dimensionless transmitted radiation vs. catalyst concentration. Tubular polished-aluminum collimator. (◇) Anatase 1, (□) Anatase 2, (△) Hombikat, (○) Degussa P25, (+) Rutile 1, (×) Rutile 2. (b) Dimensionless transmitted radiation vs. catalyst concentration. Tubular black collimator. (◇) Anatase 1, (□) Anatase 2, (△) Hombikat, (○) Degussa P25, (+) Rutile 1, (×) Rutile 2.

($R^2 > 0.98$), an apparent extinction coefficient (α) (Fig. 5a and Table 3 column 2) and the extinction coefficient (β) (Fig. 5b and Table 3 column 3) were determined for the various catalysts tested. It was observed, in this respect, that there were significant differences in β values for the various materials tested with this coefficient ranging from $8.3\,\mathrm{l\,g^{-1}}$ for Rutile 1 to $55.3\,\mathrm{l\,g^{-1}}$ for Degussa P25. In addition, the concentration required to reach 1% of P_i at the windows position is also reported in Table 3 (fourth column). Specific extinction coefficients $\left\{\beta_\mathrm{s} = \left\lfloor \beta 10^3/(R_\mathrm{w} - R_\mathrm{i}) \right\rfloor\right\}$

Table 3
Radiative flux distribution and extinction coefficients in a tubular concentric slurry reactor for various TiO_2 catalysts. $P_\mathrm{i} = 9.866 \times 10^{-6}$ einstein s^{-1}

Catalyst	α (l g^{-1})	β (l g^{-1})	C^a (g l^{-1})	β_s ($\times 10^{-4}$; cm^2 g^{-1})	P_a (%P_i)	P_bs (%P_i)
Anatase 1	39.6	44.2	0.11	1.43	71.9	−27.1
Anatase 2	22.4	26.3	0.18	0.85	57.0	−42.0
Hombikat	19.6	22.9	0.23	0.74	89.0	−10.0
Degussa P25	41.1	55.3	0.11	1.78	77.7	−21.3
Rutile 1	7.9	8.3	0.57	0.27	92.0	−7.0
Rutile 2	10.7	11.4	0.43	0.37	95.7	−3.3

[a] Defined at the conditions of transmitted radiation being 1% of the radiative flux.

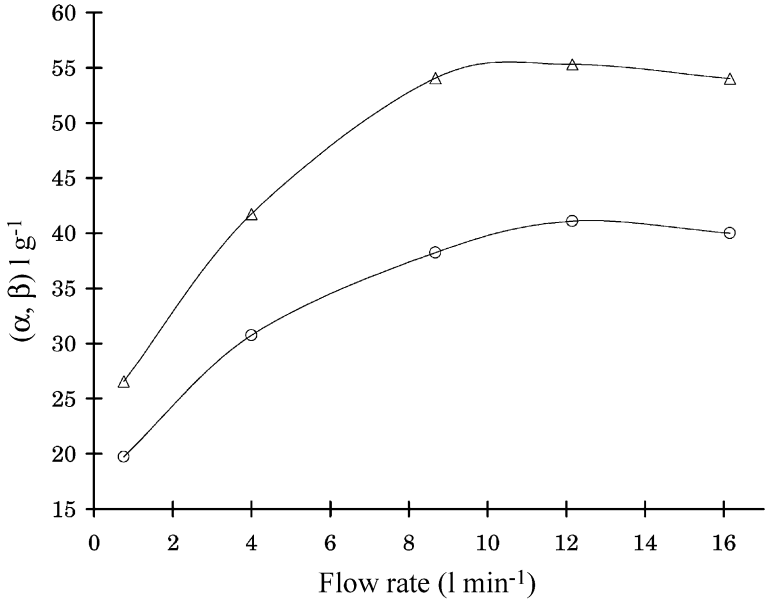

Fig. 6. Apparent extinction coefficients vs. flow rate for Degussa P25, (△) true extinction coefficient, and (○) apparent extinction coefficient.

$cm^2\,g^{-1}$ per unit of catalyst mass are also included in Table 3, with $(R_w - R_i)$ being equal to the difference between the outer surface radius of the inner cylinder and the inner surface radius of the window located in the outer cylinder. It is shown that β decreases with the particle agglomerate size and this explains the important role played by the size of the agglomerate on the extinction coefficient, with the smaller agglomerates increasing the radiation absorption-scattering and yielding larger extinction coefficient.

The effect of the flow rate on the extinction coefficients (α and β) is reported in Fig. 6 for Degussa P25. It is observed that the flow rate strongly influences the extinction coefficients with both α and β increasing with the flow rate. An almost constant value of the extinction coefficients is reached, for the reactor geometry used in this study at a flow rate of $12\,l\,min^{-1}$. Further increases in the flow rate seem to have little effect on the coefficient values. Two factors appear to be the cause for this behavior: catalyst distribution and particle agglomeration. At very low flow rates, there is uneven catalyst distribution. Catalyst is accumulated in some reactor sections being in lower concentrations in the flowing suspension. This promotes smaller extinction coefficients. At relative higher flow rates, catalyst particles are better distributed with agglomerates becoming, due to an increase in agitation, significantly smaller and yielding larger extinction coefficients. Further increases in the flow rate, above $12\,l\,min^{-1}$, however, had little effect on the extinction coefficient values.

The P_{bs} rate of back-scattered photons was determined, as described in Eq. (4), from the difference between the transmitted photons in an empty reactor and the rate of photons obtained extrapolating to $C \rightarrow 0^+$, in a P_t versus C plot, the transmitted radiation (Fig. 5a). The Last Squares method was used to generate a best-fit curve to the radiation transmittance versus concentration measurements. This curve was then used in the extrapolation to the origin and the estimation of $P_t(\theta, z)$ when $C \rightarrow 0^+$.

P_{bs}, as determined by Eq. (4), provides an estimate of the total rate of back-scattered photons exiting the system. This is supported given that photon back-scattering, for very low C, is closely related to a maximum number of back-scattering centers. Once this maximum is reached, very close to the inner cylinder, there is no additional back scattering of photons exiting the system. Experimental observations of this study reinforce this view showing that, at very low C, the transmitted power decays much faster than the typical exponential decay observed at higher solid concentrations. On the other hand, P_{bs} becomes independent of catalyst concentration when catalyst concentrations larger than $0.05\,g\,l^{-1}$ are reached. This observation held true for all catalyst considered in this study.

P_{bs} can also be expressed as a ratio of P_i as follows:

$$P_{bs} = P_i \left[\frac{q_{ac0}(\theta, z) - q_{ac}(\theta, z)|_{C_{Ci} \rightarrow 0^+}}{q_{ac0}(\theta, z)} \right] \tag{7}$$

In this respect, the rate of photons back-scattered, as determined with the method described above (from Fig. 5a and Eq. (7)) was calculated for each one of the TiO_2 catalyst. Results are reported (Table 3, column 7) as a percentage of P_i indicating that back-scattering radiation exiting the system varies for the different catalysts studied from 3.3 to 42% of P_i.

Fig. 7 reports the dimensionless radiative flux in the central axial region of the reactor for both polished-aluminum, $q_{ac}(\theta, z)/q_{ac0}(\theta, z)$, and tubular black collimator, $q_{bc}(\theta, z)/q_{bc0}(\theta, z)$, as a function of catalyst concentration for Degussa P25 at a flow rate of $12\,l\,min^{-1}$. In order to assist

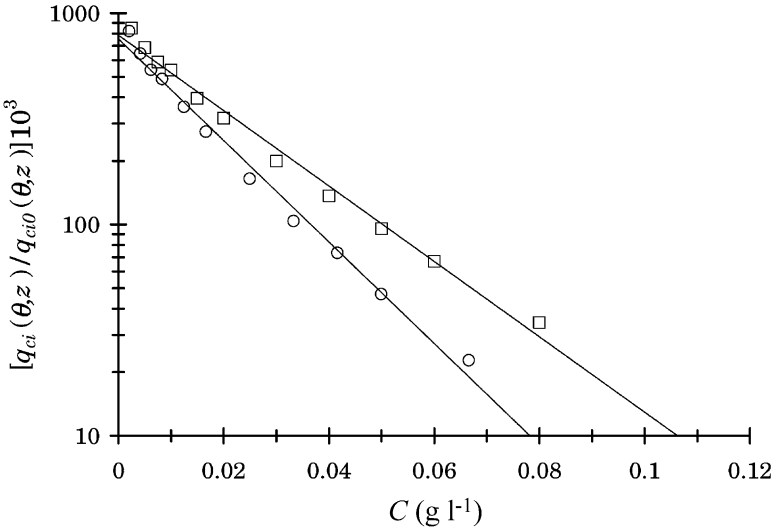

Fig. 7. Dimensionless transmitted photons (□) and transmitted non-scattered photons (○) vs. concentration for Degussa P25.

on the coefficients comparison, the readings were multiplied by a factor 1×10^3. It can be observed that there is a difference between the two exponential α and β coefficients. This difference arises given that, in the case of the polished-aluminum collimators, the forward-scattered radiation together with the transmitted non-scattered radiation reaches the detector. In the case of the black collimators, however, only the transmitted non-scattered radiation is detected. Given these facts, the β coefficients were found always greater than the α coefficients for all catalysts considered ($\beta > \alpha$, Table 3).

Regarding the rate of forward-scattered photons, P_{fs} can be calculated using the Eq. (6). In this respect, P_{fs} can be related to the transmitted photons by a difference between exponentials involving both the apparent extinction coefficient (α) and the extinction coefficient (β):

$$P_{fs} = P_t - P_{ns} = P_t|_{c\to 0^+}\left[e^{-\alpha C} - e^{-\beta C}\right]$$

Fig. 8 shows the radiative flux distribution in a Degussa P25 loaded reactor with α given in Table 3. Inner cylinder wall effects and the back scattering-radiation were also included in this simulation. This radiation distribution was specifically defined for the case of the out-coming radiation being 1% of the P_i. Moreover and in order to have a quick visualization of the catalyst effect on the radiation distribution, Fig. 8 can be compared with Fig. 3.

Fig. 9 displays the agglomerate size, d_α, versus the volume-equivalent diameter, d_p, for the various catalysts studied in this work (filled circles) and for the values reported

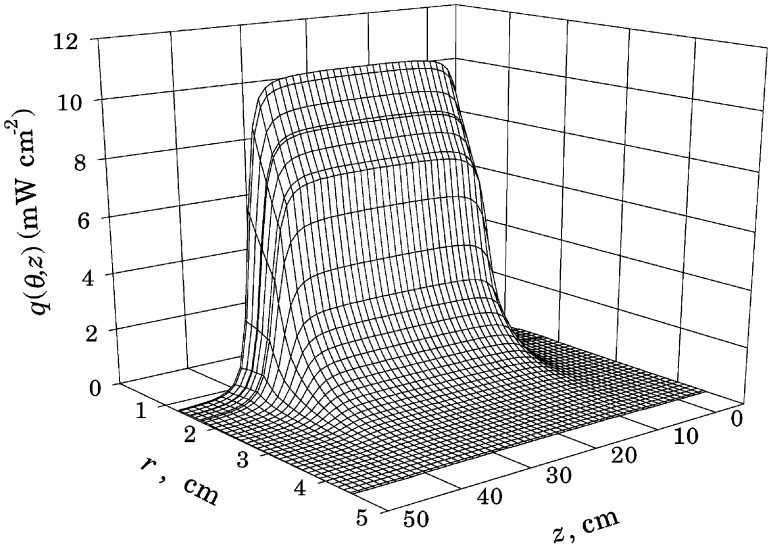

Fig. 8. Radiative flux distribution in a Degussa P25 loaded annular reactor allowing for 1% of light transmission.

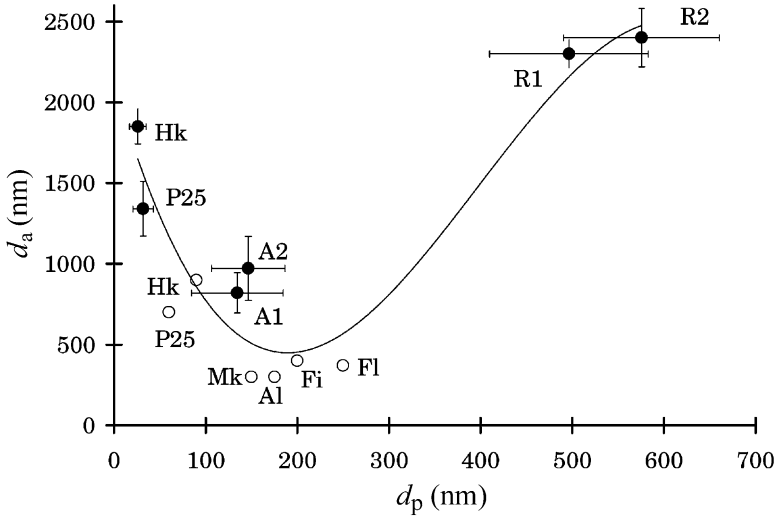

Fig. 9. Average agglomerate size vs. volume-equivalent particle diameter. Filled circles represent data from this study; open circles represent data by Cabrera et al. [5]. A1, Anatase 1; A2, Anatase 2; Al, Aldrich; Fi, Fisher; Fl, Fluka; Hk, Hombikat; Mk, Merck; P25, Degussa P25; R1, Rutile 1; R2, Rutile 2.

by Cabrera et al. [5] (open circles). Standard deviations are included as error bars for the catalysts studied. It can be observed that d_a decreases as d_p decreases until it reaches a minimum value of around 300 nm for d_p values in the range 150–300 nm. From this region and on, and as a result of an increasing influence of interparticle surface forces (presumably van der Waals' interactions) the agglomerate size starts to increase as particle diameter is further decreased.

Fig. 10 shows the extinction coefficient, β, versus the average agglomerate size, d_a for the various catalysts studied in this work (filled circles) and for the values reported by Cabrera et al. [5] (open circles). Standard deviations are included as error bars for the catalysts studied. It was found that β consistently increases as the d_a decreases. In this respect, Rutile samples exhibited lower β coefficients than the other samples since they form larger agglomerates. It has to be emphasized that the agglomerates, in the present study (filled circles in Figs. 9 and 10), satisfy the condition of being larger than two times the radiation wavelength. Thus, the principles of geometric optics can be used to describe the radiation-particle interactions and as a result, the suspension extinction coefficients are meaningful parameters to describe the radiation transmission in the TiO_2 suspensions. Under these conditions and consistent with the obtained experimental data, larger average agglomerate sizes lead to smaller irradiated cross-sectional areas per unit volume, and this yields smaller extinction coefficients.

It was observed in agreement with others [5] that agglomerate sizes and extinction coefficients are affected by sonication. For instance, as observed in this study, agglomerate

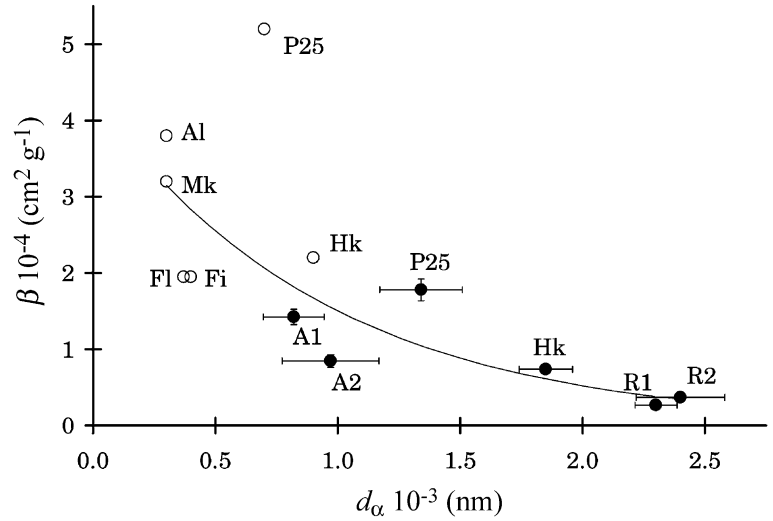

Fig. 10. Extinction coefficient vs. average agglomerate size. Filled circles represent data from this study; open circles represent data by Cabrera et al. [5]. A1, Anatase 1; A2, Anatase 2; Al, Aldrich; Fi, Fisher; Fl, Fluka; Hk, Hombikat; Mk, Merck; P25, Degussa P25; R1, Rutile 1; R2, Rutile 2.

sizes after sonication had a 0.79 μm size for Degussa P25, whereas after sonication and 1 h mixing the average agglomerate size increased to 1.34 μm. Thus, we can conclude that sonication, of the TiO_2 suspension, can play a major role in defining the agglomerate size and affecting, as a result, the suspension extinction coefficients.

5. Conclusions

The following are the significant conclusions of the present study:

(a) Radiometric measurements in a concentric tubular TiO_2 slurry reactor allowed the determination of the lamp radiation field, including axial and radial distributions of the radiative flux. Inner polished and black collimators, connecting the fused silica windows to a radiometer, helped in the determination of the rate of absorbed photons.
(b) This method specifically developed for the evaluation of the rate of absorption of photons in an aqueous TiO_2 slurry reactor allows the estimation of the total transmitted radiation, of the transmitted non-scattered radiation, and of the photon back-scattered radiation exiting the system.
(c) The total transmitted radiation and transmitted non-scattered radiation were modeled using exponential decay relationships. These decay functions incorporate extinction coefficients (α and β) and the influence of the TiO_2 concentration. It is shown that the extinction coefficient decrease with the agglomerate size with this dimension being affected by the average particle diameter.

Acknowledgements

We express our appreciation to the Consejo Nacional de Ciencia y Tecnología (CONACYT) and to the Instituto de Investigaciones Eléctricas (IIE) México for their financial support in awarding an external scholarship to Miguel Salaices. We also express our acknowledgment to the Natural Sciences and Engineering Research Council of Canada (NSERC) for the financial support of this research.

References

[1] J.C. Calvert, J.N. Pitts, Photochemistry, Wiley, New York, 1967.
[2] E.R. De Bernardez, M.A. Claria, A.E. Cassano, in: J.J. Carberry, A. Varma (Eds.), Chemical Reaction and Reactor Engineering, Marcel Dekker, New York, 26, 1987, pp. 839–921.
[3] L. Davydov, P.G. Smirniotis, S.E. Pratsinis, Novel differential reactor for the measurement of overall quantum yields, Ind. Eng. Chem. Res. 38 (1999) 1376–1383.
[4] L. Sun, J.R. Bolton, Determination of quantum yield for the photochemical generation of hydroxyl radicals in TiO_2 suspensions, J. Phys. Chem. 100 (1996) 4127–4134.
[5] M. Cabrera, O. Alfano, A.E. Cassano, Novel reactor for photocatalytic kinetic studies, Ind. Eng. Chem. Res. 93 (1994) 3031–3043.
[6] L. Palmisano, V. Augugliaro, R.J. Campostrini, A proposal for the quantitative assessment of heterogeneous photocatalytic processes, J. Catal. 143 (1993) 149–154.
[7] T.R. Serpone, D. Lawless, P. Kennepohl, G. Sauve, On the usage of turnover numbers and quantum yields in heterogeneous photocatalysis, J. Photochem. Photobiol. A, Chem. 73 (1993) 11–16.
[8] N.J. Serpone, Relative photonic efficiencies and quantum yields in heterogeneous photocatalysis, Photochem. Photobiol. A, Chem. 104 (1997) 1–12.
[9] B. Serrano, H.I. de Lasa, Photocatalytic degradation of water organic pollutants. Kinetic modeling and energy efficiency, Ind. Eng. Chem. Res. 36 (1997) 4705–4711.
[10] J. Bolton, S. Carter, Homogeneous photodegradation of pollutants in contaminated water: an introduction, in: G. Hels, R. Zeep, D. Crosby (Eds.), Aquatic and Surface Photochemistry, Lewis Publications, 1994, p. 467.
[11] M. Lindner, D.W. Bahnemann, B.J. Hirthe, Solar water detoxification: novel TiO_2 powders as high active photocatalyst, J. Solar Energy Eng. 119 (1997) 120–125.
[12] X. Nanping, S. Zaifeng, F. Yiqun, D. Junhang, S. Jun, Z.C.H. Michael, Effects of particle size of TiO_2 on photocatalytic degradation of methylene blue in aqueous suspensions, Ind. Eng. Chem. Res. 38 (1999) 373–379.
[13] V. Augugliaro, V. Loddo, L. Palmisano, Performance of heterogeneous photocatalytic systems: Influence of operational variables on photoactivity of aqueous suspension of TiO_2, J. Catal. 153 (1995) 32–40.
[14] A.C. Martin, M.A. Baltanas, A.E. Cassano, Photocatalytic reactors. Part I. Optical behavior of TiO_2 particulate suspensions, J. Photochem. Photobiol. A, Chem. 76 (1993) 199–208.
[15] V. Augugliaro, L. Palmisano, L.M. Schiavello, Photon absorption by aqueous TiO_2 dispersion contained in a stirred photoreactor, AIChE J. 37 (1991) 1096–1100.
[16] O.M. Alfano, M.I. Cabrera, A.E. Cassano, Modeling of light scattering in photochemical reactors, Chem. Eng. Sci. 49 (1994) 5327–5346.
[17] M. Salaices, B. Serrano, H.I. de Lasa, Photocatalytic conversion of organic pollutants. Extinction coefficients and quantum efficiencies, Ind. Eng. Chem. Res. 40 (2001) 5455–5464.
[18] R. Siegel, J.R. Howell, Thermal Radiation Heat Transfer, 3rd Edition, Vol. 12, Hemisphere, Bristol, PA, 1992.
[19] R. Tsekov, P.G. Smirniotis, Radiation field in continuous annular photocatalytic reactors: role of the lamp finite size, Chem. Eng. Sci. 52 (1997) 1667–1671.
[20] M. Schiavello, V. Augugliaro, L. Palmisano, An experimental method for the determination of the photon flow reflected and adsorbed by aqueous dispersions containing polycrystalline solids in heterogeneous photocatalysis, J. Catal. 127 (1991) 332–341.